

Structure and ferromagnetic instability of the oxygen-deficient SrTiO₃ surface

Soham S. Ghosh⁽¹⁾ and Efstratios Manousakis^(1,2)

⁽¹⁾ *Department of Physics and National High Magnetic Field Laboratory,
Florida State University, Tallahassee, FL 32306-4350, USA*

⁽²⁾ *Department of Physics, University of Athens,
Panepistimioupolis, Zografos, 157 84 Athens, Greece*

(Dated: November 25, 2015)

Abstract

SrTiO₃ (STO) is the substrate of choice to grow oxide thin-films and oxide heterojunctions, which can form quasi-two-dimensional electronic phases that exhibit a wealth of phenomena¹⁻⁶, and, thus, a workhorse in the emerging field of metal-oxide electronics^{7,8}. Hence, it is of great importance to know the exact character of the STO surface itself under various oxygen environments. Using density functional theory within the spin generalized gradient approximation we have investigated the structural, electronic and magnetic properties of the oxygen-deficient STO surface. We find that the surface oxygen vacancies order in periodic arrays giving rise to surface magnetic moments and a quasi two-dimensional electron gas in the occupied Ti 3-d orbitals. The surface confinement, the oxygen-vacancy ordering, and the octahedra distortions give rise to spin-polarized t_{2g} dispersive sub-bands; their energy split near the Brillouin zone center acts as an effective Zeeman term, which, when we turn on a Rashba interaction, produces bands with momentum-spin correlations similar to those recently discovered on oxygen deficient STO surface⁹.

The interface between two transition metal oxides forms quasi-two dimensional electronic phases^{10–13} that exhibit a rich set of phenomena, including tunable insulator-superconductor-metal transitions^{1,2}, large magnetoresistance³, ferromagnetism³ and superconductivity^{4–6}. The perovskite SrTiO₃ (STO) is the substrate used for many such heterojunctions, and, therefore, it plays a crucial role in the area of metal-oxide interfaces^{7,8}. Although it is a non-magnetic wide-band-insulator in bulk with a band-gap of 3.2 eV¹⁰, a quasi two-dimensional electron gas (Q2DEG) with interesting spin-momentum correlations has been detected on its surface^{9,14–17}. This Q2DEG can be produced through multiple methods, such as gating^{2,18}, by creating surface oxygen vacancies^{14,15} or by inserting a δ -doped layer^{19–22} inside the bulk crystal.

As seen by angle-resolved photoemission spectroscopy (ARPES), the Q2DEG has a strongly confined component made up of two sub-bands, separated from each other by about 90 meV, forming concentric circular sections of the Fermi surface (FS)^{14,17}, and a relatively less strongly confined component, about 200 meV higher in energy, forming ellipsoidal sections of the FS¹⁵. Ab-initio^{23,24} and model^{25,26} calculations have identified Ti t_{2g} as the host states, though there are open questions about the nature of the Q2DEG. The two concentric rings of the FS on the k_x - k_y plane are made up of $3d_{xy}$ orbitals, and two ellipsoids aligned along the k_x and k_y directions are $3d_{xz}/d_{yz}$ states in nature¹⁵. The $3d_{xz}/d_{yz}$ states are quasi one dimensional, and as seen from layer-by-layer ARPES study²⁷ on LaTiO₃/SrTiO₃ interface, they have bulk-like behavior. These FS features have been seen to be created by intense ultraviolet irradiation¹⁷. They persist under varying levels of oxygen vacancies and annealing conditions¹⁵, and, thus, seem ubiquitous.

At Titanate interfaces with a polar perovskite, such as LaAlO₃, it has been suggested²⁸ that oxygen vacancies (Ov) create magnetic moments through orbital reconstruction and e_g occupancy, thereby modifying the occupied electronic levels produced by the so-called polar catastrophe. Oxygen-deficient STO in bulk has been discovered to contain optically induced magnetic moments¹⁶, and the magnetism inverts sign upon switching between right- and left-circular polarization. Recently, a spin- and angle-resolved photoemission spectroscopy (SARPES) study⁹ has shown that the concentric circular bands have a gap at the Γ point, opposite spin chirality and a large value of split at the Fermi surface that cannot be explained by a purely Rashba-like model. It was suggested that this state breaks the time-reversal symmetry⁹, and an argument in favor of an antiferromagnetic ground state as the

result of one of the instabilities of the 2D Fermi liquid with exchange interactions has been presented²⁹.

In this paper, through a fully-relaxed spin-unconstrained DFT study of (001) terminated STO slabs with various surface oxygen vacancy patterns, we show that stable periodic arrays of oxygen vacancies can form in a surface TiO_2 layer and cause the spin-degeneracy of the occupied sub-bands to be lifted at the GGA level giving rise to a weakly ferromagnetic ground state. By considering slabs with multiple surface oxygen vacancy configurations (such as those of Fig. 1 and those discussed in Supplementary Note 1) and various surface Ov densities n_v ($= 1/4, 1/6$, and $1/8$), we find that for a given surface Ov density, the superstructure in which the surface oxygen vacancies order in periodic stripe arrays, such as the one in Fig. 1, is characterized by the lowest energy. In addition, Fig. 2 shows the particular striped ordered vacancy configuration which is the most stable within an allowed range of oxygen chemical potential. Furthermore, the Ti atoms of the top-layer and the layer just below it acquire stable magnetic moments below surface Ov density of $n_v = 1/8$ (refer to Supplementary Material Table S1) producing an internal Zeeman field, in which the level of doping and the surface magnetic moments are functions of surface Ov density. At the Γ point, the Q2DEG is spread over multiple layers and hosted by spin-non-degenerate states several hundred meV below the Fermi level. These deeper occupied states near the zone-center, which are strongly $3d_{xy}$ in character, host a Q2DEG but contribute a relatively small part to the net magnetic moment, most of which is localized on the Ti atoms at the oxygen-deficient surface away from the zone center, and hosted by a reconstructed mixture of t_{2g} and e_g . Last, these findings via ab initio calculations are strongly supported by the following results. Taking into account a Rashba interaction in the x-y plane, we find that these spin-split bands near the zone center acquire the spin-momentum correlations recently discovered⁹ by a SARPES study. The zone center gap is enhanced by the introduction of a Coulomb U term via a GGA+U calculation, but the qualitative features of the spin-chirality and the momentum-spin correlations of the bands in the direction parallel to the surface, as well as the bands themselves near the Γ point are reproduced. The spin chirality perpendicular to the surface is attributed to a matrix element of the SARPES process.^{9,30}

The Q2DEG in STO has been associated with a band bending of ~ 300 meV near the surface^{14,17}. Confinement in this potential-well lifts the degeneracy between the $3d_{xy}$ of different Ti atoms and produces a series of light parabolic sub-bands split in energy, which

produce concentric rings on the Fermi surface near the zone center, once doped. Oxygen vacancy doping lifts the spin-degeneracy in each of these bands but by different magnitudes, as shown in Fig. 3. We find that four STO-layer and six STO-layer slabs have qualitatively similar band structure (this is illustrated in Fig. S2 of Supplementary Material), hence we believe that our results and conclusions presented here, which are obtained from slabs containing only four STO-layers, may be applicable to the semi-infinite system. At $1/6$ surface Ov density, these states are as far deep as 400 meV below the Fermi level at the Γ point. Their site and Y_{lm} -projection (refer to Supplementary Material Note 3) illustrate that each of the spin-split pair of the light sub-bands has a preference for a Ti orbital belonging to a different TiO_2 layer. This is an effect of the confining potential-well that quantizes levels in the (001) direction. Around the Γ -point, they are all $3d_{xy}$, except the heavy sub-bands ~ 50 meV below the Fermi surface, which are largely $3d_{xz}$. At the GGA level, there are multiple spin pair bands (see Fig. 3 and Supplementary Material Fig. S3) that have significant contribution from the Ti atoms immediately below the oxygen deficient surface, and within the range of a SARPES experiment. However, as we illustrate in the Supplementary Material (Fig. S4), addition of an on-site Hubbard Coulomb- U term causes the electrons to repel each other and move away from the surface, leaving all but one pair within the range of the SARPES probe. This pair of bands associated with atoms near the TiO_2 surface has a zone-center splitting of ~ 29 meV at the GGA level and ~ 80 meV at the GGA+ U ($U = 2$ eV) level.

By switching on the spin-orbit coupling (SOC) in the system, we find a slightly modified near- Γ band structure for the four STO-layer slab, as shown in the Supplementary Material Fig. S5. The change in the $3d_{xy}$ bands around the Γ point is negligible. The biggest effect of SOC can be seen in lifting the degeneracy of the band-crossing at the corners, as expected. It preserves the net magnetic moment at the surface and the spin-polarization of the $3d_{xy}$ bands around the Γ point. At this mean-field level, SOC effect is predictably small enough so that the spin-orbit mixing changes the spin-eigenstates only by a small amount and the spin up-down characterization remains valid. The most important role of the spin-orbit coupling is that it simply selects the direction of the effective internal “Zeeman field” (which splits our lowest energy bands within our GGA-spin calculation) to be perpendicular to the orbital angular momentum $x - y$ plane.

Fig. 4 shows the total density of states (DOS) of a four STO-layer slab along with the

integrated up and down DOS as a function of energy as well as the orbital projected DOS of one of the Ti atoms at the surface at the GGA level. We find that in the absence of a Rashba term and at $1/6$ Ov surface density, the low-lying $3d_{xy}$ bands near the zone-center carry finite but small amounts of magnetic moments. Most of the contribution to the magnetic moment comes from heavier sub-bands away from the zone-center, and depend on a reconstruction of the e_g states. As we can observe in Fig. 4, the spin-polarized e_g states of the Ti atom next to a missing oxygen is pulled below the Fermi level and get mixed with the t_{2g} states. On the other hand, the occupied bands of the Ti atoms one layer below the surface are entirely t_{2g} in nature with almost non-magnetic $3d_{xy}$ states (refer to Supplementary Material Fig. S6).

The splitting of the e_g states and their mixing with the t_{2g} states give the surface Ti atoms a magnetic moment (with magnetic moments for the two nonequivalent surface Ti atoms given by $M_{Ti(1)} = 0.118\mu_B$ and $M_{Ti(2)} = 0.228\mu_B$) each for $n_v = 1/6$.

The band picture shown in Fig. 3 does not take into consideration the Rashba effect, which couples spin with momentum. In the existence of strong fields caused by surface termination and oxygen vacancy, inversion symmetry is lost and the octahedra buckle, causing previously forbidden hopping channels to open. This, coupled with a strong spin-orbit coupling²⁶ produces a prominent planar Rashba effect. For the Ti atom one unit-cell below the oxygen deficient surface, this effect can be modeled using a simple 2-D Hamiltonian for small values of \mathbf{k} . Written in the basis of Ti $3d_{xy}$ Bloch states and S_z eigenstates, the Hamiltonian is:

$$\hat{H} = \epsilon_{GGA}(\vec{k})\hat{1} - \alpha(\sigma_x k_y - \sigma_y k_x) - h\sigma_z, \quad (1)$$

where α is the Rashba parameter, σ_x , σ_y and σ_z are Pauli matrices, $\hat{1}$ is the unit matrix, and the last term is the Zeeman term due to an effective internal mean field in the z-direction which is responsible for the spin-splitting the bands which we found by allowing for spin- and lattice relaxation within the GGA and GGA+U. In the absence of an external magnetic field, both magnetic directions along the z-axis are equally likely, and we use $h = \pm|h|$ to account for ferromagnetic domains that average to zero in a macroscopic measurement like SARPES⁹. Here $\epsilon_{GGA}(\vec{k})$ is the band structure obtained as the average between the lowest two near-surface bands closer to the oxygen deficient TiO_2 surface obtained in our DFT calculation which correspond to spin-up and spin-down states, and the value of this field will be chosen to reproduce the energy splitting of these two lowest bands. In addition, $\epsilon_{GGA}(\vec{k})$ is very close (apart from a constant) to the results of our DFT calculation when we

do not include spin. The eigenvalues of this Hamiltonian are

$$e_{\pm}(k) = \epsilon_{GGA}(\vec{k}) \pm |h|\Delta(k); \quad \Delta(k) = \sqrt{1 + \gamma^2 k^2}. \quad (2)$$

where $k^2 = k_x^2 + k_y^2$ and $\gamma = \alpha/|h|$. The corresponding expectation values of the spin components are as follows:

$$\begin{pmatrix} \langle \pm | \sigma_x | \pm \rangle \\ \langle \pm | \sigma_y | \pm \rangle \\ \langle \pm | \sigma_z | \pm \rangle \end{pmatrix} = \mp \frac{1}{\Delta(k)} \begin{pmatrix} \gamma k_y \\ -\gamma k_x \\ \frac{h}{|h|} \end{pmatrix}. \quad (3)$$

In Fig. 5 we compare the experimentally determined bands to those obtained using Eq. 2 by choosing the parameters in the following way. Fig. 5(a) shows the result of our fit of the experimentally determined x-component of the spin to the form given by Eq. 3 where the only fitting parameter is γ . The solid line is the result of our fit with $\gamma = 17.045 \text{ \AA}$. Fig. 5(b) is obtained using $h = 14.55 \text{ meV}$ as found by our spin GGA calculation and the value of $\gamma = 17.045 \text{ \AA}$ determined by the previously discussed fit. This implies that the Rashba parameter is 248 meV \AA for the given value of h .

Fig. 5(c) is obtained using $h = 40.0 \text{ meV}$ as found in GGA+U calculation for a four STO-layer slab and $\alpha = 300 \text{ meV \AA}$, illustrating a better agreement of the zone-center gap and the momentum dispersion of the bands with experiment.

We note that there is a possibility that SARPES overestimates the spin polarization by not accurately estimating the quasiparticle spectral weight away from the peak of the spectral function: it is clear that the quasiparticle function is widely spread around the peak and, thus, the part of the spectral weight away from the peak can hide under the contribution of tails from other nearby bands. In such case the estimation of the Rashba parameter can be significantly affected.

The photo-excitation process itself mixes states with different angular momentum components, which depend on the light polarization, causing a rotation of the electron spin-polarization through the spin-orbit coupling term. Thus, the expectation value $\langle \sigma_z \rangle$ picks up a contribution proportional to $\langle \sigma_x \rangle$ and/or to $\langle \sigma_y \rangle$. In the absence of an external magnetic field, the average value of the term proportional to h over the entire surface is expected to be zero. This can explain that the expectation value of $\langle \sigma_z \rangle$ measured in the SARPES study has a k -dependence similar to that of $\langle \sigma_x \rangle$ or $\langle \sigma_y \rangle$.

In conclusion, we find that our ab initio calculations predict very interesting patterns of Ov ordering on the (001) STO surface which lead to a small ferromagnetic moment of the surface Ti atoms. Furthermore, major experimental characteristics of the STO surface can be qualitatively reproduced by a GGA (and GGA+U) spin calculation where we have included the effects of the planar Rashba coupling. The underlying symmetry breaking and the presence of a quantum-well potential near the surface give rise to discrete energy bands in the (001) direction. When surface oxygen vacancies are introduced and the structure is relaxed within a spin-dependent GGA, bands near the TiO_2 surface emerge characterized by a dispersion near the zone center similar to that observed by recent SARPES studies. More importantly, we find that the fully relaxed GGA calculation opens a spin-gap at the zone center, which is further enhanced by adding a moderate U in a GGA+U calculation. The contribution to the magnetic moments come primarily from the neighborhood of the S and X points in the BZ, and localized at the reconstructed t_{2g} and e_g of the Ti atoms at the oxygen deficient surface (Supplementary Material Fig. S7). At the spin-GGA level and at the present high levels of doping, the system is weakly ferromagnetic. Therefore, it is reasonable to assume a theoretical framework whereby we identify with these $3d_{xy}$ bands those seen in the most recent SARPES study⁹. Then by taking these bands as a starting point we turned on a planar Rashba term, the lowest lying, closest to the TiO_2 surface $3d_{xy}$ bands qualitatively reproduce the experimental SARPES results⁹ for the energy bands close to the Γ point. Furthermore, they reproduce the momentum-spin correlations in the x and y directions seen in SARPES and they have no net magnetic moment in the $x - y$ plane.

I. METHODS

We consider slabs between four and six STO-layer thick, terminated in the (001) direction by an SrO surface on one end and an oxygen-deficient TiO_2 surface on the other. Such a system lacks a plane of inversion around the $x - y$ plane. The presence of surfaces in the (001) direction of our slab geometry creates an electrostatic potential which has one minima near the oxygen deficient TiO_2 surface, and another near the TiO_2 layer on the opposite end. We focus on the dispersive bands localized close to the oxygen deficient surface and within the depth-range of the ARPES study.

All computations were performed using the plane-wave basis set (plane wave cutoff of

540 eV) with the projector augmented wave (PAW) methodology³¹ used to describe the wavefunctions of the core electrons, as implemented in the VASP package^{32–35}. The Perdew-Burke-Ernzerhof (PBE) exchange correlation functional³⁶ was used for all GGA calculations. The 4*s* and 3*d* electrons of the transition metal atom and the oxygen 2*s* and 2*p* electrons were treated as valence electrons. An initial unit cell length of 3.944 Å was used, which was found by curve-fitting the ground state energies of bulk STO to find the minimum. The Brillouin zone was sampled with a maximum of $5 \times 15 \times 1$ k-point mesh for the self-consistent cycles³⁷. Forces were converged to less than 10 meV/Å for each ion. A local Coulomb repulsion of Ti 3*d* electrons was accounted within GGA+U approach with $U_{\text{Ti}} = 2$ eV.

II. ACKNOWLEDGMENTS

The authors would like to thank C. S. Hellberg for useful communication. This work was supported in part by the U.S. National High Magnetic Field Laboratory, which is partially funded by the NSF DMR-1157490 and the State of Florida.

-
- ¹ Thiel, S., Hammerl, G., Schmehl, A., Schneider, C. W. & Mannhart, J. Tunable quasi-two-dimensional electron gases in oxide heterostructures. *Science* **313**, 1942–1945 (2006).
 - ² Ueno, K. *et al.* Electric-field-induced superconductivity in an insulator. *Nat Mater* **7**, 855–858 (2008).
 - ³ Brinkman, A. *et al.* Magnetic effects at the interface between non-magnetic oxides. *Nat Mater* **6**, 493–496 (2007).
 - ⁴ Reyren, N. *et al.* Superconducting interfaces between insulating oxides. *Science* **317**, 1196–1199 (2007).
 - ⁵ Li, L., Richter, C., Mannhart, J. & Ashoori, R. C. Coexistence of magnetic order and two-dimensional superconductivity at LaAlO₃/SrTiO₃ interfaces. *Nat Phys* **7**, 762–766 (2011).
 - ⁶ Bert, J. A. *et al.* Direct imaging of the coexistence of ferromagnetism and superconductivity at the LaAlO₃/SrTiO₃ interface. *Nat Phys* **7**, 767–771 (2011).
 - ⁷ Ramirez, A. P. Oxide electronics emerge. *Science* **315**, 1377–1378 (2007).

- ⁸ Cen, C., Thiel, S., Mannhart, J. & Levy, J. Oxide nanoelectronics on demand. *Science* **323**, 1026–1030 (2009).
- ⁹ Santander-Syro, A. F. *et al.* Giant spin splitting of the two-dimensional electron gas at the surface of SrTiO₃. *Nat Mater* **13**, 1085–1090 (2014). Letter.
- ¹⁰ Ohtomo, A. & Hwang, H. Y. A high-mobility electron gas at the LaAlO₃/SrTiO₃ heterointerface. *Nature* **427**, 423–426 (2004).
- ¹¹ Hwang, H. Y. *et al.* Emergent phenomena at oxide interfaces. *Nat Mater* **11**, 103–113 (2012).
- ¹² Cen, C. *et al.* Nanoscale control of an interfacial metal-insulator transition at room temperature. *Nat Mater* **7**, 298–302 (2008).
- ¹³ Mannhart, J. & Schlom, D. G. Oxide interfaces—An opportunity for electronics. *Science* **327**, 1607–1611 (2010).
- ¹⁴ Santander-Syro, A. F. *et al.* Two-dimensional electron gas with universal subbands at the surface of SrTiO₃. *Nature* **469**, 189–193 (2011).
- ¹⁵ Plumb, N. C. *et al.* Mixed dimensionality of confined conducting electrons in the surface region of SrTiO₃. *Phys. Rev. Lett.* **113**, 086801 (2014).
- ¹⁶ Rice, W. A. D. *et al.* Persistent optically induced magnetism in oxygen-deficient strontium titanate. *Nat Mater* **13**, 481–487 (2014). Article.
- ¹⁷ Meevasana, W. *et al.* Creation and control of a two-dimensional electron liquid at the bare SrTiO₃ interface. *Nat Mater* **10**, 114–118 (2011).
- ¹⁸ Lee, Y. *et al.* Phase diagram of electrostatically doped SrTiO₃. *Phys. Rev. Lett.* **106**, 136809 (2011).
- ¹⁹ Kim, M. *et al.* Fermi surface and superconductivity in low-density high-mobility δ -doped SrTiO₃. *Phys. Rev. Lett.* **107**, 106801 (2011).
- ²⁰ Kozuka, Y. *et al.* Two-dimensional normal-state quantum oscillations in a superconducting heterostructure. *Nature* **462**, 487–490 (2009).
- ²¹ Kozuka, Y. *et al.* Enhancing the electron mobility via delta-doping in SrTiO₃. *Applied Physics Letters* **97**, – (2010).
- ²² Jalan, B., Stemmer, S., Mack, S. & Allen, S. J. Two-dimensional electron gas in δ -doped SrTiO₃. *Phys. Rev. B* **82**, 081103 (2010).
- ²³ Shen, J., Lee, H., Valentí, R. & Jeschke, H. O. *Ab initio* study of the two-dimensional metallic state at the surface of SrTiO₃: Importance of oxygen vacancies. *Phys. Rev. B* **86**, 195119

(2012).

- ²⁴ Popović, Z. S., Satpathy, S. & Martin, R. M. Origin of the two-dimensional electron gas carrier density at the LaAlO_3 on SrTiO_3 interface. *Phys. Rev. Lett.* **101**, 256801 (2008).
- ²⁵ Khalsa, G. & MacDonald, A. H. Theory of the SrTiO_3 surface state two-dimensional electron gas. *Phys. Rev. B* **86**, 125121 (2012).
- ²⁶ Khalsa, G., Lee, B. & MacDonald, A. H. Theory of t_{2g} electron-gas rashba interactions. *Phys. Rev. B* **88**, 041302 (2013).
- ²⁷ Chang, Y. J. *et al.* Layer-by-layer evolution of a two-dimensional electron gas near an oxide interface. *Phys. Rev. Lett.* **111**, 126401 (2013).
- ²⁸ Pavlenko, N., Kopp, T. & Mannhart, J. Emerging magnetism and electronic phase separation at titanate interfaces. *Phys. Rev. B* **88**, 201104 (2013).
- ²⁹ Gor'kov, L. P. Antiferromagnetism of two-dimensional electronic gas on light-irradiated SrTiO_3 and at LaAlO_3 / SrTiO_3 interfaces. *Journal of Physics: Condensed Matter* **27**, 252001 (2015).
- ³⁰ Mirhosseini, H., Flieger, M. & Henk, J. Dirac-cone-like surface state in $\text{w}(110)$: dispersion, spin texture and photoemission from first principles. *New Journal of Physics* **15**, 033019 (2013).
- ³¹ Blöchl, P. E. Projector augmented-wave method. *Phys. Rev. B* **50**, 17953 (1994).
- ³² Shishkin, M., Marsman, M. & Kresse, G. Accurate quasiparticle spectra from self-consistent GW calculations with vertex corrections. *Phys. Rev. Lett.* **99**, 246403 (2007).
- ³³ Fuchs, F., Furthmüller, J., Bechstedt, F., Shishkin, M. & Kresse, G. Quasiparticle band structure based on a generalized kohn-sham scheme. *Phys. Rev. B* **76**, 115109 (2007).
- ³⁴ Shishkin, M. & Kresse, G. Self-consistent GW calculations for semiconductors and insulators. *Phys. Rev. B* **75**, 235102 (2007).
- ³⁵ Shishkin, M. & Kresse, G. Implementation and performance of the frequency-dependent GW method within the paw framework. *Phys. Rev. B* **74**, 035101 (2006).
- ³⁶ Perdew, J. P., Burke, K. & Ernzerhof, M. Generalized gradient approximation made simple. *Phys. Rev. Lett.* **77**, 3865 (1996).
- ³⁷ Monkhorst, H. J. & Pack, J. D. Special points for brillouin-zone integrations. *Phys. Rev. B* **13**, 5188–5192 (1976).

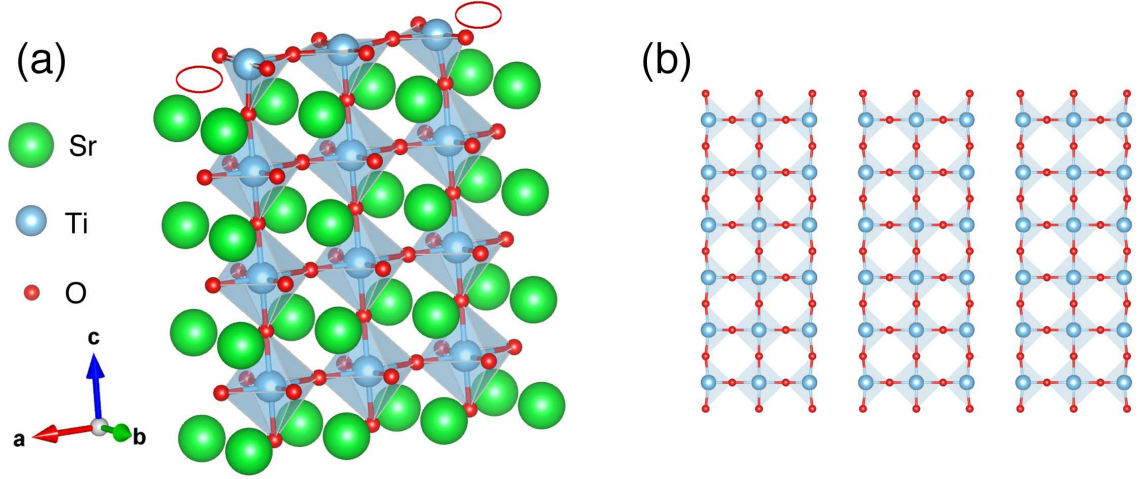


FIG. 1. (color-online) (a) Four layers of atomically relaxed STO bounded in the (001) direction by an SrO surface on one side and a TiO₂ surface on the other side with an imposed $1/6$ surface Ov coverage. The presence of the oxygen vacancies (the sites of which are denoted by the two red circles) cause the tetrahedra at the TiO₂ surface to buckle and push both the O and the Ti atoms away from the lower layers. The Ti-Ti bond length at the surface is larger by about 0.3 \AA along the x-axis as compared to that along the y-axis. (b) Top surface head-on view of the superlattice structure of oxygen vacancy ordering in periodic arrays.

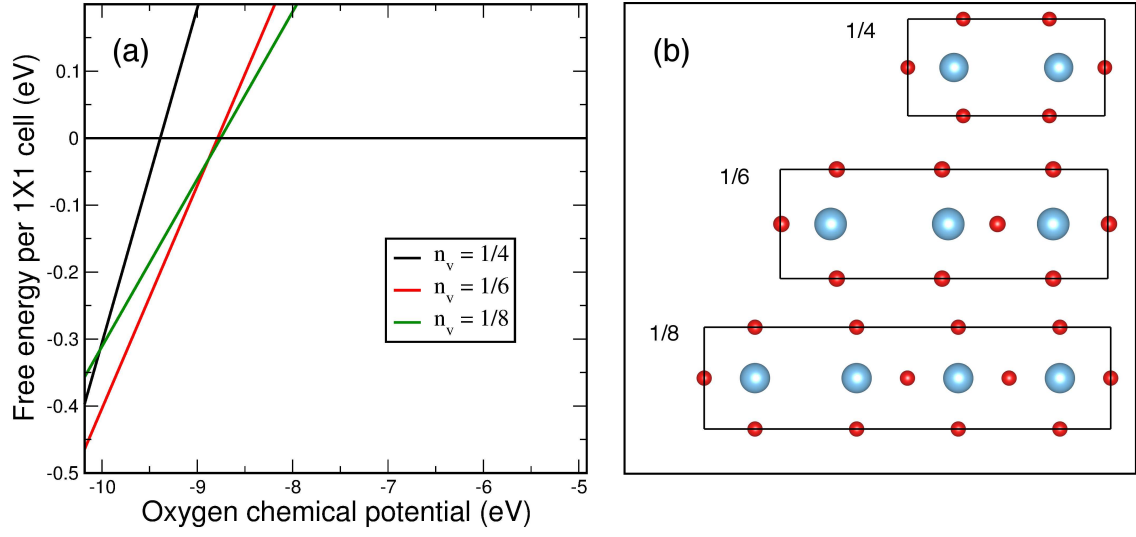


FIG. 2. (color-online)(a) Stability graph of the striped vacancy pattern discussed in Fig.1 with different surface Ov densities. All three densities produce similar sub-surface $3d_{xy}$ bands near the zone-center but differ in the magnitude of the magnetic moments. For an explanation of the free energy and the allowed range of oxygen chemical potential see Supplementary Material Note 6. (b) Top view of the various $\text{Ti}_{(m)}\text{O}_{(n)}$ units at the TiO_2 surface with one oxygen vacancy per u.c., showing (i) a 2×1 u.c. with one eliminated O atom at (0.50, 0.50) creating a stripe of missing oxygen atoms along the y-axis (Ov surface density $n_v = 1/4$) and giving each Ti atom exactly one nearest neighbor vacancy, (ii) a 3×1 u.c. with one eliminated O at (0.33, 0.50) causing a similar vacancy stripe but with lower density ($n_v = 1/6$), and (iii) a 4×1 u.c. with one eliminated O at (0.25, 0.50), creating vacancy stripes with a Ov surface density of $n_v = 1/8$. Further vacancy configurations are discussed in the Supplementary Material.

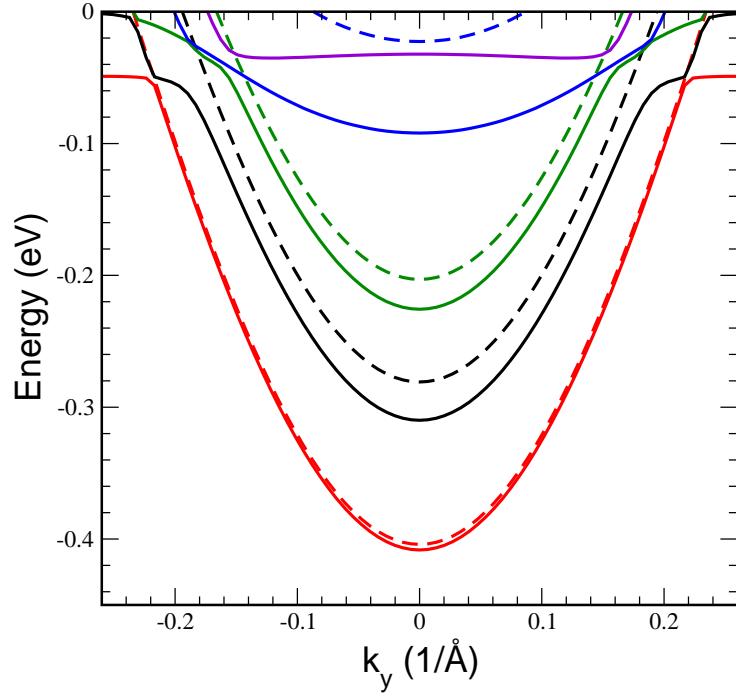


FIG. 3. (color-online) The near- Γ spin-GGA band structure of the STO slabs with striped vacancy configuration ($n_v = 1/6$). Up-spins bands are denoted with solid lines and corresponding down-spin bands denoted with dashed lines. The $3d_{xy}$ bands are light and dispersive, while the $3d_{xz}$ and the $3d_{yz}$ are heavier and less dispersive due to confinement in the z-direction, which also produces the observed level quantization of states.

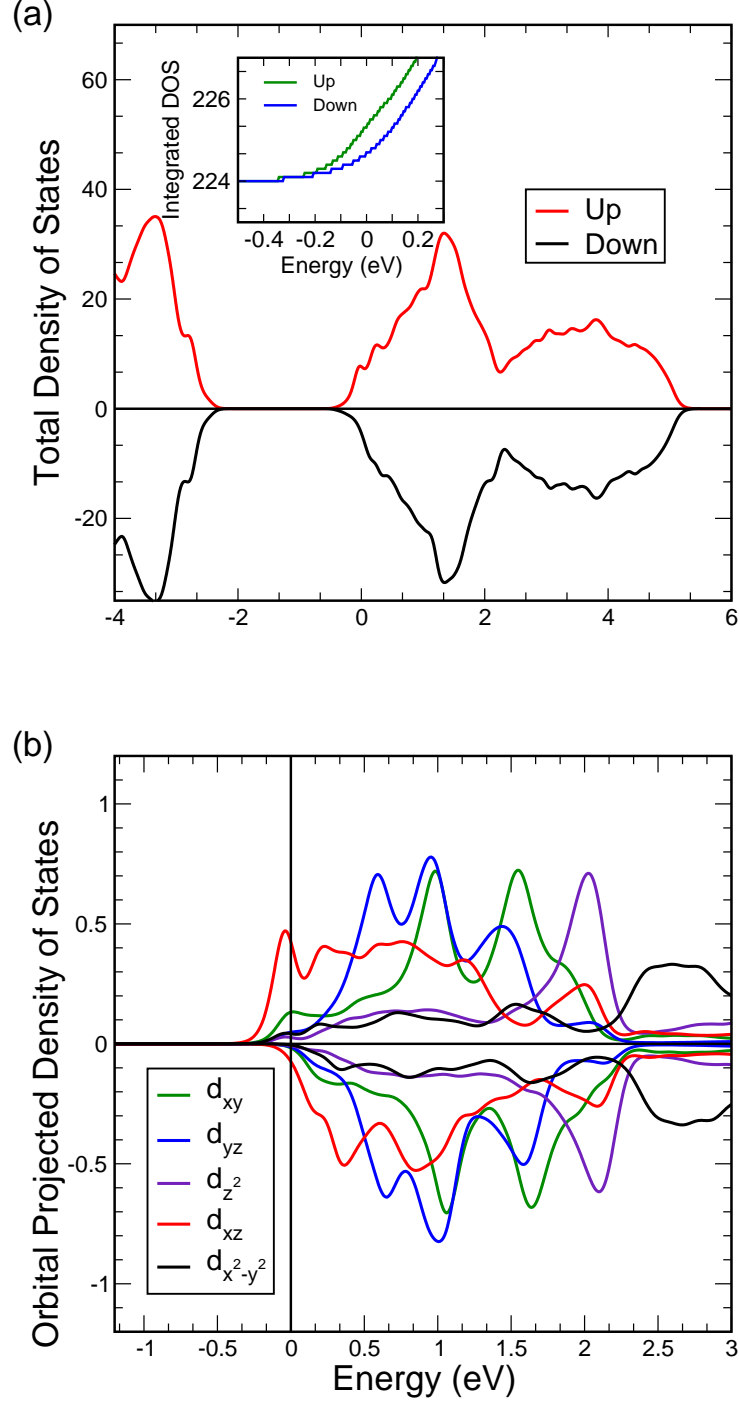


FIG. 4. (color-online) (a) Total up and down DOS of a four STO-layer slab with $1/6$ Ov surface density at the TiO_2 surface. The zero is the Fermi level at the present level of doping. (inset) Integrated up and down dos, showing the onset of magnetism at ~ 300 meV below the Fermi level. (b) Projected DOS of the 3d orbitals of a surface Ti atom next to an oxygen vacancy. The occupied polarized states are a mixture of spin-polarized t_{2g} and e_g located around the S-point of the BZ.

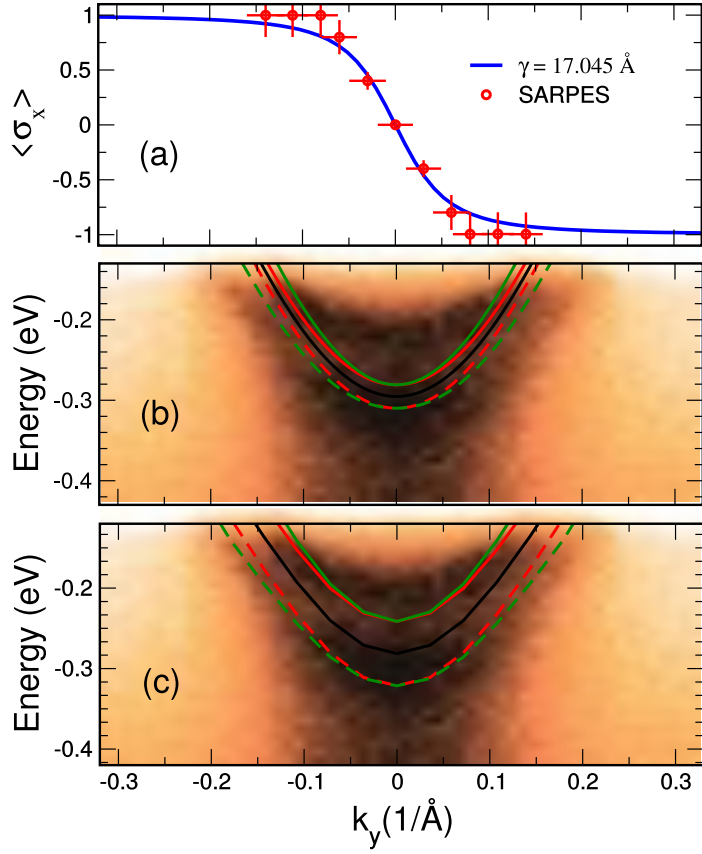


FIG. 5. (color-online) (a) The result of fitting the experimentally determined⁹ spin x-component to the form given by Eq. 3 indicating a large planar Rashba coupling near the surface. (b) The near-surface GGA bands of the four STO-layer slab after applying a Rashba spin-split term using Eq. 2 as compared to the experimental results⁹. (c) The same as in (b) using the bands by GGA+U. The black solid line is the result of GGA or GGA+U without spin-relaxation. The green and red solid (dashed) lines are obtained with GGA or GGA+U after spin-relaxation for down (up) with and without the Rashba interaction respectively.

Supplementary Material

for the paper entitled

Structure and ferromagnetic instability of oxygen-deficient SrTiO_3 surface

Soham S. Ghosh¹ and Efstratios Manousakis^{1,2}

⁽¹⁾ *Department of Physics and National High Magnetic Field Laboratory,
Florida State University, Tallahassee, FL 32306-4350, USA*

⁽²⁾ *Department of Physics, University of Athens,
Panepistimioupolis, Zografos, 157 84 Athens, Greece*

(Dated: November 25, 2015)

I. SUPPLEMENTARY NOTE 1: OTHER VACANCY CONFIGURATIONS

Fig. S1 shows the vacancy configurations considered here which are not shown in the main part of the paper associated with Fig. 1. The non-stripe configurations are higher in energy by ~ 0.5 eV (for $n_v = 1/4$) per supercell used in the DFT calculations than the stripe configuration. The $(1/4)$ stripe and dimer configurations have stable magnetic moments at the spin-GGA level while the $(1/8)$ stripe and 2×1 configurations have no noticeable magnetic moments. In Table S1 we list the magnetic moments of the surface and sub-surface Ti atoms for the systems under consideration. For the stripe configuration with $n_v = 1/4$, the two surface Ti atoms have similar environment and equal magnetic moments. For $n_v = 1/6$, the Ti atoms next to the Ov has less magnetic moment than the Ti with all nearest neighbor oxygen atoms present.

II. SUPPLEMENTARY NOTE 2: THE SEMI-INFINITE APPROXIMATION

To argue that a four STO-layer slab is enough to capture the semi-infinite-ness of the experimental samples, we show in Fig. S2 the near zone-center bands of a four STO-layer and a six STO-layer slabs for $n_v = 1/4$. The six STO-layer slab has more subbands of d_{xy} character, but most of these are away from the depth-range of SARPES (as demonstrated in Fig. S4 for five STO-layer slabs), and the band structure near the Fermi level is the same between the four and six STO-layer slabs. We therefore believe that the results obtained from four STO-layer thick slabs may be valid for the semi-infinite system.

III. SUPPLEMENTARY NOTE 3: ORBITAL- AND SITE-PROJECTION OF BANDS

In Fig. S3 the orbital and site-projection of the lowest four spin-pairs of bands around the Γ point and along k_y for the four STO-layer slab with $n_v = 1/4$ is illustrated with band 1 being the deepest pair. The colors signify the orbital character of the band (red = d_{xy} , green = d_{xz}) and the unit cell along the horizontal axis is a reference to the Ti site-location of these states inside the unit cell. A Coulomb U in the form of GGA+ U repels the spins from one another in real space and causes the spin-pairs to spread, as a result of which the up-spin and the down-spin bands are nested on neighboring Ti atoms, and the spin-gap is widened. We demonstrate this in Fig. S4 which illustrates the near- Γ orbital and site projection of the deepest corresponding occupied bands around the Γ -point for a five STO-layer slab ($n_v = 1/4$) slab (using $U = 4$ eV and $J = 1$ eV).

IV. SUPPLEMENTARY NOTE 4: SPIN-ORBIT COUPLING

In Fig. S5 we give the results obtained by switching on the spin-orbit coupling (SOC) in a four STO-layer slab with $n_v = 1/4$. As can be seen, we get a slightly modified near- Γ band structure as compared to Fig. S2 where the SOC was neglected. The effect of SOC is found to be maximum where the bands cross each other, as expected. It preserves the net magnetic moment at the surface and the spin-polarization of the d_{xy} bands around the Γ point.

V. SUPPLEMENTARY NOTE 5: DENSITY OF STATES OF THE Ti ATOM ONE LAYER BELOW THE SURFACE

In contrast to the surface Ti atoms whose occupied states are a mix of t_{2g} and e_g , the projected density of states in the Ti atom one layer below the surface (Fig. S6) with $n_v = 1/6$ shows far less polarization, with its occupied states being predominantly t_{2g} in character and located near the zone-center. Here the magnetic moment is an order of magnitude less than that on the surface, and most of the polarization is in the d_{xz} state.

VI. SUPPLEMENTARY NOTE 6: STABILITY OF OXYGEN VACANCIES

The possible range of Oxygen chemical potential μ_O can be determined by first noting that the value is bounded from above by the chemical potential of the triplet O_2 molecule,

$$\mu_O < \mu_{O_2}/2 = -4.917\text{eV}. \quad (\text{S.1})$$

Furthermore, it is constrained by the relation

$$\mu_{Sr} + \mu_{Ti} + 3\mu_O = \mu_{SrTiO_3}^{bulk} = -40.125\text{eV}, \quad (\text{S.2})$$

where the chemical potentials of Sr and Ti must themselves satisfy inequality constraints:

$$\mu_{Sr} < \mu_{Sr}^{bulk} = -1.6840\text{eV}, \quad (\text{S.3})$$

$$\mu_{Ti} < \mu_{Ti}^{bulk} = -7.8981\text{eV}. \quad (\text{S.4})$$

Therefore the allowable energy of the oxygen chemical potential is

$$-10.181\text{eV} < \mu_O < -4.917\text{eV}. \quad (\text{S.5})$$

The free-energy per unit cell plotted in Fig. 2 for each oxygen deficient structure is taken to be

$$F = [F_V - F_0 + \mu_0]/N_u, \quad (\text{S.6})$$

where F_V is the free-energy of the oxygen deficient structure, F_0 is the free-energy of the no-vacancy structure and N_u is the number of 1×1 unit cells needed to make the supercell used in our DFT.

All three structures are stable at only very low oxygen chemical potential in equilibrium. Therefore, we believe that non-equilibrium effects like intense UV irradiation is necessary to create oxygen vacancies with the density required for the spin-split.

Ov type(n_v)	stripe(1/4),	stripe(1/6), Ti(1)	stripe(1/6),Ti(2)	stripe(1/8)	dimer	2×1 chain
surface	0.391	0.118	0.228	0.000	0.368	0.000
1 layer deep	0.046	0.030	0.069	0.000	0.033	0.000

TABLE S1. Magnetic moments of surface Ti atoms and of those one layer below the surface, in units of μ_B . For $n_v = 1/6$, Ti(1) refers to the atom closest to the O vacancy, and Ti(2) refers to the atom farther away.

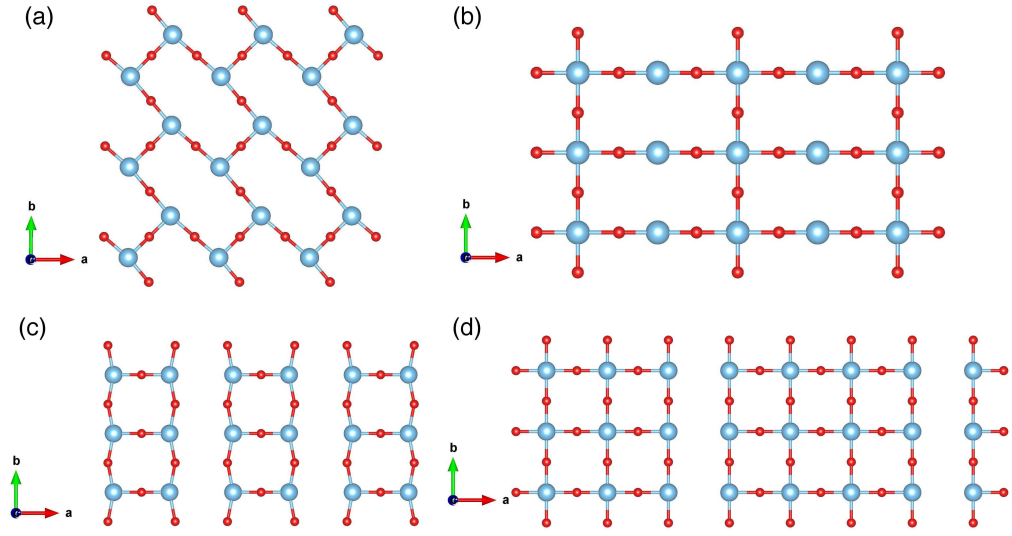


FIG. S1. (color-online) (a) A four STO-layer slab with $\sqrt{2} \times \sqrt{2}$ (dimerized) vacancies, causing each surface Ti to have one nearest neighbor vacancy. (b) A 2×1 configuration with chains of vacancies in the y -direction. The configuration (b) contains two different types of surface Ti, one with no nearest neighbor vacancies, and the other with two nearest neighbor vacancies. Both configurations have doping level $n_v = 1/4$ (25%). (c) Stripe configuration, $n_v = 1/4$ and (d) stripe configuration, $n_v = 1/8$.

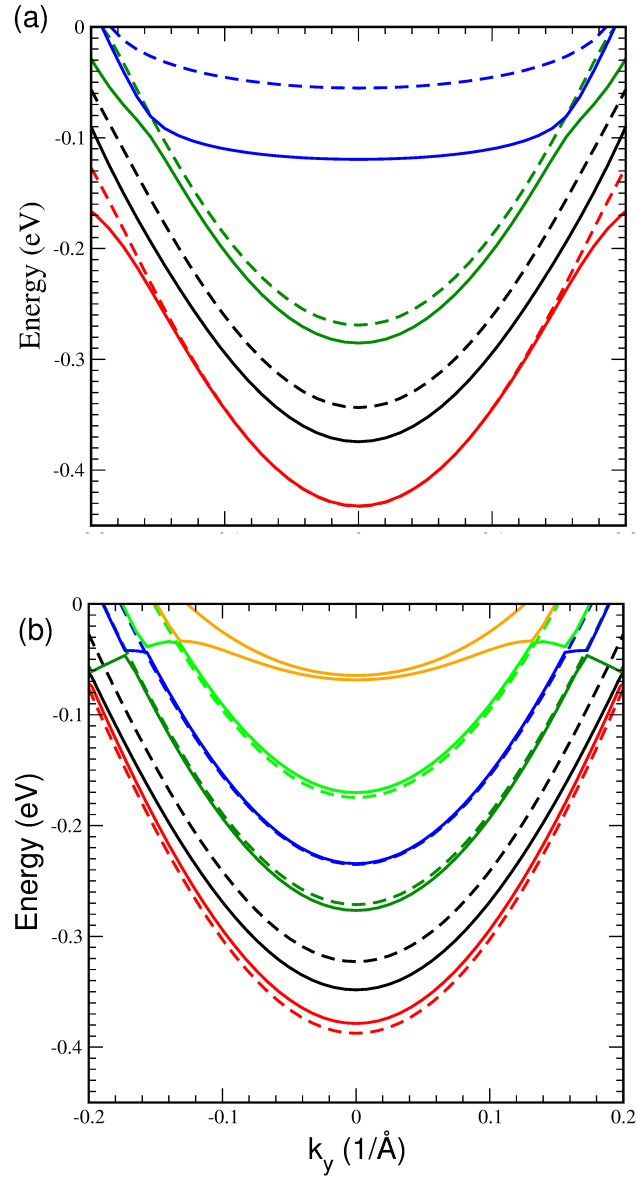


FIG. S2. (color-online) Comparison of the near zone-center conduction bands of oxygen-deficient (a) 4 layer STO and (b) 6 layer STO with $n_v = 1/4$. Up-spin bands are denoted by solid lines and down-spin bands by corresponding dashed lines. The spin-split is maximum for the bands near the Ov surface and reduces as we go deeper into the bulk.

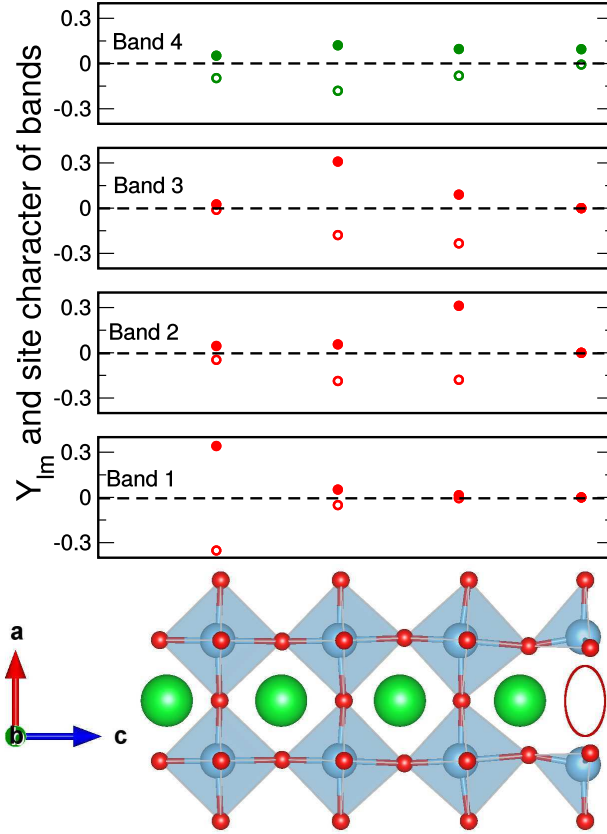


FIG. S3. (color-online) Orbital and site-projection of the lowest 4 spin-pairs of bands of a 4 layer STO slab ($n_v = 1/4$) around the Γ point and along k_y , with band 1 being the deepest pair. The site locations are shown by the crystal unit cell aligned along the horizontal axis. On the graph, red is d_{xy} and green is d_{xz} . Up-spin is above the axis and is shown in filled circles whereas down-spin is below the axis and is shown in empty circles. The position of the missing oxygen on the surface is shown with a red circle. Each d_{xy} can be seen to be localized more on a distinct TiO_2 plane. The deepest pair of bands is Ti d_{xy} near the SrO surface and the next deepest pair is Ti d_{xy} next to the TiO_2 surface. The d_{xz} band can be seen to be more de-localized than the d_{xy} .

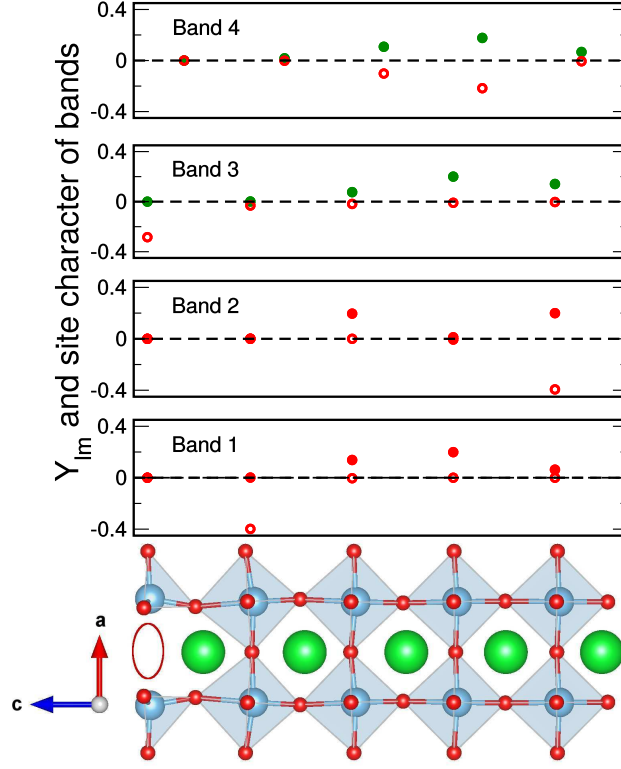


FIG. S4. (color-online) Orbital and site-projection of the lowest 4 spin-pairs of bands of a 5 layer STO slab ($n_v = 1/4$) around the Γ point and along k_y , with band 1 being the deepest pair. A GGA+U scheme has been used. The site locations are shown by the crystal unit cell aligned along the horizontal axis. On the graph, red is d_{xy} and green is d_{xz} . The position of a missing oxygen on the surface is shown with a red circle. The Coulomb term causes the spins in a pair to move away from each other in real space, but the quantization effect of the confining potential is maintained. Up-spin is above the axis and is shown in filled circles whereas down-spin is below the axis and is shown in empty circles.

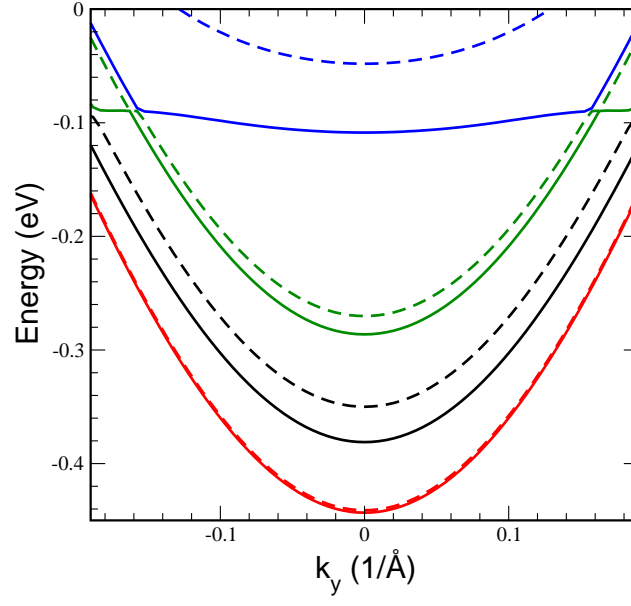


FIG. S5. (color-online) The near- Γ band structure of the oxygen-deficient 4 layer STO ($n_v = 1/4$) with spin-orbit coupling included. Up-spins are denoted with solid lines and down-spins denoted with dashed lines. The change in the d_{xy} bands around close to the Γ point is negligible. The biggest effect of SOC can be seen in lifting the degeneracy of the band-crossing at the corners.

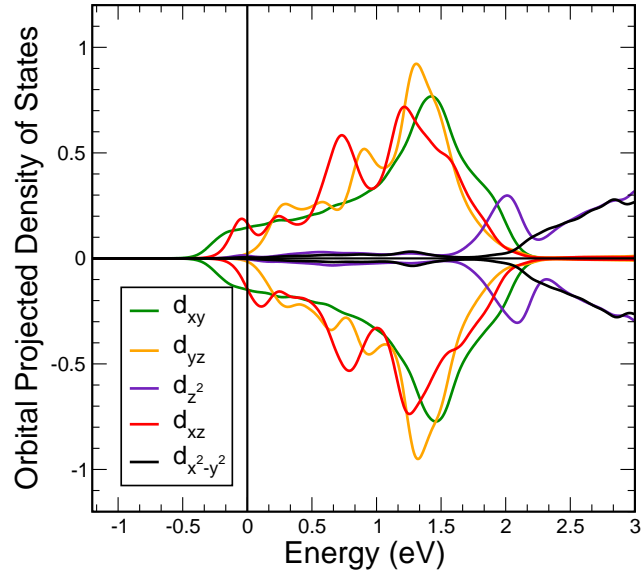


FIG. S6. (color-online) DOS of the 3d states of a Ti atom one layer below the oxygen-deficient TiO_2 surface ($n_v = 1/6$). The occupied states around the zone-center are t_{2g} in nature. At this GGA-level, the d_{xy} states carry negligible magnetic moments, and most of the spin-polarization is in the d_{xz} state.

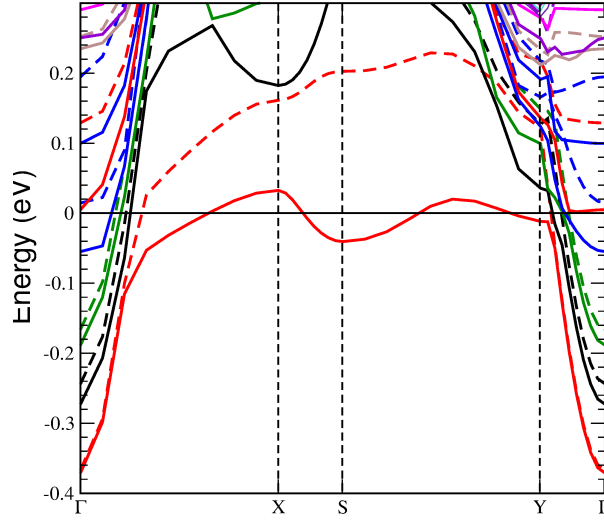


FIG. S7. (color-online) The planar BZ band structure of the oxygen-deficient four STO-layer slab with $n_v = 1/6$. Up-spins are denoted with solid lines and down-spins denoted with dashed lines. The lowest occupied pair of spin bands is degenerate near the Γ point and is contributed by the Ti atoms away from the oxygen deficient TiO_2 surface. The second lowest spin-split pair comes from the Ti atoms one layer below the oxygen deficient TiO_2 surface, which are the bands of interest. The majority of the magnetic moment comes from the BZ corner and edge where the states are localized on the doped TiO_2 surface as a mixture of t_{2g} and e_g with a considerable spin-split.